Journal Name

ARTICLE TYPE

Cite this: DOI: 00.0000/xxxxxxxxxx

A flat-lying dimer as a key intermediate in NO reduction on Cu(100)

Kenta Kuroishi[a]‡, Muhammad Rifqi Al Fauzan[b,e]‡, Thanh Ngoc Pham[b], Yuelin Wang[b], Yuji Hamamoto[b], Kouji Inagaki[b], Akitoshi Shiotari[a]¶, Hiroshi Okuyama*[a], Shin-ichiro Hatta[a], Tetsuya Aruga[a], Ikutaro Hamada[b,c], Yoshitada Morikawa,[b,c,d]

Received Date
Accepted Date

DOI: 00.0000/xxxxxxxxxx

The reaction of nitric oxide (NO) on Cu(100) is studied by scanning tunneling microscope, electron energy loss spectroscopy and density functional theory calculations. The NO molecules adsorb mainly as monomers at 64 K, and react and dissociate to yield oxygen atoms on the surface at ∼70 K. The temperature required for the dissociation is significantly low at Cu(100), compared to those at Cu(111) and Cu(110). The minimum energy pathway of the reaction is via the $(NO)_2$ formation, which converts to a flat-lying ONNO and then dissociates into N_2O and O with a considerably low activation energy. We propose that the formation of $(NO)_2$ and flat-lying ONNO is the key to the exceptionally high reactivity of NO on Cu(100).

1 Introduction

The adsorption and reaction of nitric oxide on metal surfaces have been studied extensively for understanding the catalytic reduction processes of NO_x emitted from combustion engine. The single-crystalline metal surfaces were often used as model catalysts, where the key processes involved in the reaction has been argued at a molecular level.[1–14] The reduction of NO at low temperatures was proposed to be mediated by the formation of NO dimer [$(NO)_2$] as $2NO(ad) \rightarrow (NO)_2(ad) \rightarrow N_2O(g) + O(ad)$ in the early experiments[4,5,7,10,11] and theories[15,16]. King and co-workers thoroughly studied the reaction process of NO on Ag(111) by using infrared reflection absorption spectroscopy (IRAS),[17,18] near-edge x-ray absorption spectroscopy (NEXAFS),[18] scanning tunneling microscope (STM),[19] and density functional theory (DFT) calculations.[20] The $(NO)_2$ forms in the submonolayer regime at 60 K and reacts to yield N_2O and oxygen atom on the surface at ∼80 K.[17] The structure of $(NO)_2$ was proposed to be tilted with the N-N axis oriented along the surface and the molecular plane tilted from the surface normal by ∼30°.[18] Furthermore, the DFT calculation revealed that the $(NO)_2$ is converted into O-down geometry.[20] This inverted $(NO)_2$ was proposed to be a precursor to the dissociation, but was not identified by the experiments, probably due to its short lifetime.

The interaction of NO with Au and Ag surfaces is weak so that $(NO)_2$ forms and mediates the dissociation, while that with d-metal surfaces are relatively strong so that direct dissociation occurs.[2] Therefore it is of fundamental interest to investigate the interaction with Cu surfaces which is intermediate between the two cases. In addition, Cu clusters were recently proposed to be promising for selective catalytic reduction of NO,[21] attracting industrial interest as well. The adsorption and reaction of NO on Cu(111) was studied by IRAS.[11] At initial coverage at 88 K, the internal stretch mode was observed, indicating that NO adsorbs in a molecular form. It was later found that the molecules adsorb in units of trimer by using STM[22] and EELS.[23] The molecular state was observed up to 170 K,[11] suggesting that the N-O bond rupture is activated at higher temperature than 170 K on Cu(111). The reaction of NO on Cu(110) was studied by IRAS,[12] and by STM and electron energy loss spectroscopy (EELS).[24] The molecules adsorb as a monomer in a flat configuration, as verified by STM at 78-90 K and EELS at 110 K. Upon heating, the NO

[a] Department of Chemistry, Graduate School of Science, Kyoto University, Kyoto 606-8502, Japan. E-mail: hokuyama@kuchem.kyoto-u.ac.jp
[b] Department of Precision Engineering, Graduate School of Engineering, Osaka University, 2-1, Yamadaoka, Suita, Osaka 565-0871, Japan.
[c] Elements Strategy Initiative for Catalysts and Batteries (ESICB), Kyoto University, Goryo-Ohara, Nishikyou-ku, Katsura, Kyoto 615-8245, Japan
[d] Research Center for Precision Engineering, Graduate School of Engineering, Osaka University, 2-1 Yamadaoka, Suita, Osaka 565-0871, Japan
[e] Department of Electrical Engineering and Informatics, Vocational College, Universitas Gadjah Mada, Yogyakarta 55281, Indonesia
†Electronic Supplementary Information (ESI) available: [details of any supplementary information available should be included here]. See DOI: 10.1039/cXCP00000x/
‡These authors contributed equally to this work.
¶ Present address: Department of Physical Chemistry, Fritz-Haber Institute of the Max-Planck Society, Faradayweg 4-6, 14195 Berlin, Germany.

molecules dissociate at ∼140 K,[24] in agreement with the result of IRAS.[12] Thus, the N-O dissociation is activated above 100 K at low coverage on Cu(111) and Cu(110). It is noted that the dissociation occurs at lower temperature (85 K) with increasing coverage where physisorbed $(NO)_2$ forms and may act as a precursor to the dissociation.[12]

The adsorption and reaction of NO on Cu(100) was studied by Kim et al. by using IRAS.[3] Upon adsorption at ∼25 K, they observed monomer species at low coverage, and the dimer species dominates with increasing coverage. Upon heating to 78 K, vibrational signature of N_2O was observed, indicating the onset of the N-O bond rupture. Therefore, the dissociation is facile on Cu(100), as compared to that on Cu(111) and Cu(110), suggesting that the microscopic surface structure plays a crucial role in the reaction of NO.

In this work, we investigated the reaction of NO at Cu(100) mainly by using STM and DFT, and observed that NO dissociates to yield oxygen atom on the surface at ∼70 K. Our DFT calculations reveal that the reaction proceeds via $(NO)_2$ and ONNO in a flat-lying configuration. The flat-lying ONNO is identified by STM, and proposed to be a key intermediate that facilitates the reaction of NO on Cu(100).

2 Methods

The experiments were conducted in an ultrahigh vacuum (UHV) chamber equipped with an STM (Unisoku, USM-1200). A single crystalline Cu(100) was cleaned by repeated cycles of argon ion sputtering and annealing. The clean Cu(100) surface was exposed to NO gas via a tube doser positioned at ∼1 cm in front of the sample surface. An electrochemically etched W or PtIr tip was used as an STM probe. The STM images were acquired in constant current mode at the sample bias V_s=0.1 V and tunneling current I= 5 nA, unless otherwise mentioned. The experiments were conducted at 6 K and 64-78 K with liquid helium and liquid/solid nitrogen, respectively. For the latter, liquid nitrogen was evacuated to vaporize and condense, achieving a minimum temperature of 64 K. The reaction of the molecules was induced by STM as follows: The tip was positioned over the molecule at V_s=0.1 V and I= 5 nA. Then the feedback was turned off and V_s=0.25 V was applied for 5 s. The tunnel current was monitored during the voltage pulse, which showed abrupt change when the reaction occurred.

The EELS was conducted in another UHV chamber equipped with a high-resolution electron energy loss spectrometer (LK-5000, LK Technologies, Inc.). The base pressure of the chamber was below 1×10^{-10} Torr. For the EELS measurements, the incidence angle of θ_i=60°, reflection angle of θ_r=60° from the surface normal, and energy resolution of 2-3 meV (the full-width at half-maximum of the elastic peak) were used. The primary energy of electron (E_p) of 5 eV was used. The mean free path of electron in solids decreases as the kinetic energy increases up to ∼50 eV[25,26]. This indicates that higher E_p is preferential for the surface sensitivity. On the other hand, the cross section of excitation decreases with E_p in the dipole scattering regime under the present condition, $(\hbar\omega/2E_p)\approx0.01$[27]. Actually, the loss intensity normalized to that of elastic peak was not so much changed with E_p. Therefore, we chose the E_p so that the elastic peak intensity was maximized.

The Cu(100) surface was exposed to NO, ^{15}NO, or N^{18}O gas via a tube doser (positioned ∼1 cm from the surface) through a variable-leak valve. Exposures were calculated by multiplication of the background NO pressure by time and by magnification factor (600) of the doser,[23] and are given in units of L (1 L=1×10^{-6} Torr s).

The DFT calculations were performed using the STATE package,[28,29] which has been successfully used to study the interaction between molecules and metal surfaces,[30–33] including NO on Cu(110)[34] and Cu(111).[35] Electron-ion interactions were described by using the ultrasoft pseudopotentials.[36] The plane-wave basis set was used to expand wave functions and charge density with cutoff energies of 36 Ry and 400 Ry, respectively. We used optB86b-vdW[37] functional as implemented[38–40] in the STATE package.

The Cu(100) surface was modeled by a slab composed of four atomic layers and a vacuum of ∼ 30 Å thickness, which was periodically repeated in the surface lateral directions. An optimized lattice constant of Cu (3.610 Å) was used to construct the slab. A (4×3) supercell was used. A uniform 5×6 k-point grid was used to sample the surface Brillouin zone. Geometry optimization was performed by keeping the bottommost layer fixed at the bulk position, while the remaining degrees of freedom were fully relaxed until the forces became less than 5×10^{-2} eV/Å. For the gas-phase NO molecule, spin polarization was considered. On the other hand, spin moment of the NO molecules is lost upon adsorption,[41] similar to the cases of Cu(110) and Cu(111) surfaces.[34,35] Thus, we did not take into account the spin polarization for the adsorption systems.

The nudged elastic band (NEB)[42] and the climbing image nudged elastic band (CI-NEB)[43] were used to explore the minimum energy paths of the NO dissociation. We confirmed that the transition state was properly located by performing the vibrational analyses and veryfining that there was a single imaginary frequency mode in the vibrational spectrum. The vibrational analysis was performed by using the finite difference method by considering only the adsorbates and leaving the metal slab fixed. The approach was confirmed valid in our previous study.[35] The zero-point energy correction was included in the evaluation of the activation energies.

Electronic structure analyses, namely, density of states and crystal orbital overlap population (COOP),[44–46] and STM simulations based on the Tersoff-Hamann theory[47,48] were performed by using a four-layer (5×5) slab with a Γ-centered 6×6 k-point set. Geometry optimization was also performed independently, by using similar setting to that for the (4×3) supercell.

3 Results and discussion

3.1 Experimental observation of NO dissociation

Figure 1 shows a typical STM image of Cu(100) at 6 K after the surface was exposed to NO gas at 10 K. An image of bare Cu(100) surface in the inset shows atomic corrugation and thus indicates the crystallographic direction along the surface. Such images

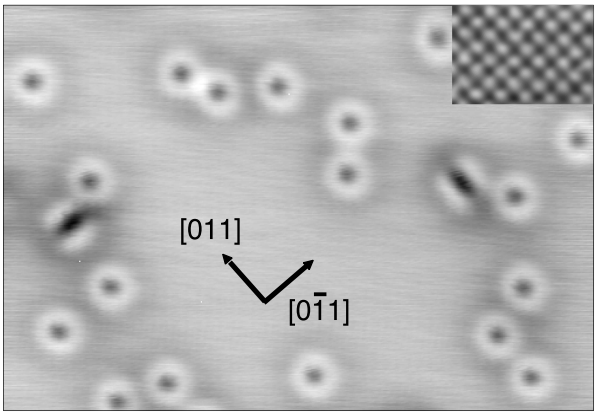

Fig. 1 A typical STM image of NO/Cu(100) at low temperature. The surface was exposed to NO gas at 10 K and imaged at 6 K. The ring-shaped protrusions are attributed to the degenerate $2\pi*$ orbital of upright NO monomers. Twin protrusions are assigned to the NO dimer [a_0-$(NO)_2$]. The image size is 89×58Å. The inset shows the image of Cu(100) obtained with a molecular tip.

were obtained when the apex of the tip was modified by some molecular species. The NO molecules adsorb upright at the hollow sites and appear as ring-shaped protrusions representing the degenerate $2\pi^*$ molecular orbital.[41] The elongated twin protrusions were also observed, which are ascribed to two NO molecules at the nearest-neighbor (a_0=2.56 Å) hollow sites and denoted by a_0-$(NO)_2$.

The molecules are immobile at 6 K but activated to migrate on the surface as the temperature increases, as shown by the time-lapse STM images obtained at 64 K (Figs. 2a-c). The mobile molecules were encountered to form a a_0-$(NO)_2$ (arrow in Fig.2b), but detached afterward (Fig. 2c), suggesting that the dimer is not thermodynamically stable compared to the monomers even at 64 K. This is in contrast to the case of NO on Cu(111), where the molecules preferentially assemble to form a trimer at similar temperatures.[22,23,49]

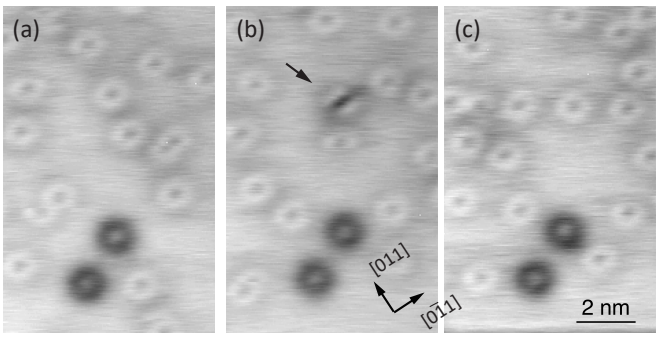

Fig. 2 (a)-(c) Sequential STM images of NO/Cu(100) at 64 K at an interval of 60 s. The NO monomers (bright rings) are migrating across the surface, and a a_0-$(NO)_2$ is temporally formed as indicated by the arrow in (b). The two dark rings in the bottom are immobile impurities used as markers. The images were obtained at V_s=0.1 V and I= 2 nA.

The time-lapse images obtained at 68 K are shown in Figs. 3a and b. The diffusion rate at this temperature was so high that individual molecules were hardly observed. Instead, dark spots were observed as a result of the reaction of NO, as indicated by the arrow in Fig. 3b. Most of the molecules were reacted and dark spots dominated on the surface after the temperature increased to 85 K (Fig. 3c). It is noted that a minority of unreacted NO molecules remained on the surface, as shown by the dotted arrow in Fig. 3c. The unreacted molecules can be confirmed to exist in the large-scale image (Fig. S1).

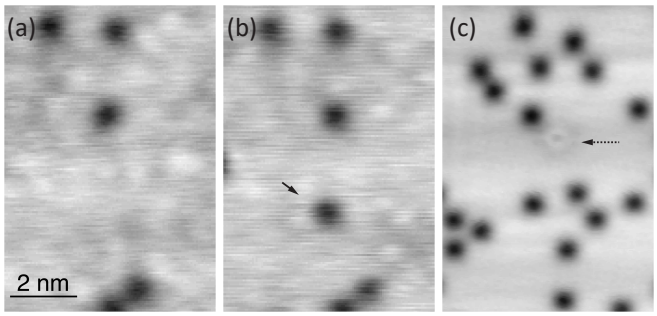

Fig. 3 (a),(b) Sequential STM images of NO/Cu(100) at 68 K at an interval of 60 s. The diffusion of NO molecules is so fast that the bright rings (see Fig. 2) are hardly observed. Instead, the dark spots appear as a result of the reaction of NO, as shown by the arrow in (b). (c) STM image obtained after the surface temperature was increased to 85 K and then decreased to 64 K. The dark spots dominate, but minority molecular NO still remains, as shown by a dotted arrow. The images (a) and (b) were obtained at V_s=0.1 V and I= 1 nA, and (c) at V_s=0.1 V and I= 2 nA.

To identify the chemical nature of the reaction products (dark spots in the STM image), we recorded EEL spectra of Cu(100) as a function of exposure to NO at 100 K (Fig. 4). Here, we focus mainly on the initial exposure to compare with the result of STM. At the initial stage of the exposure (0.3 L), the spectra showed a single peak at 44 meV. We observed no peak due to the N-O stretch mode which would appear at 150-220 meV if NO existed on the surface in a molecular form[50]. The absence of the internal mode indicates that the NO molecules dissociate at low coverage. The 44 meV peak is associated with the dark spots in the STM image. From the isotope shift of the 44 meV peak (Fig. 4, inset), it is assigned to the O-Cu stretch mode. This assignment is supported by DFT calculation, in which the stretching modes for ^{16}O and ^{18}O on the Cu(100) surface are calculated to be 45 meV and 43 meV, respectively. The single peak suggests that the N atoms are absent on the surface. This is consistent with the observation by IRAS that N_2O and O atom were produced upon heating the surface to 78 K in the monolayer regime.[3] The former (N_2O) may desorb at 100 K in the present EELS experiment. Thus, NO adsorbs in a molecular form at 64 K, and dissociates at ∼68 K to yield O atoms on the surface, while N atoms may desorb from the surface as N_2O or N_2. With increasing the exposure, the EEL spectra showed additional peaks at 52, 97 and 156 meV. The latter two were assigned to the bending and N-O stretching modes of adsorbed N_2O, respectively, in the previous EELS study[6]. The 52 meV peak is newly observed and possibly assigned to the O-Cu stretch mode of adsorbed N_2O.

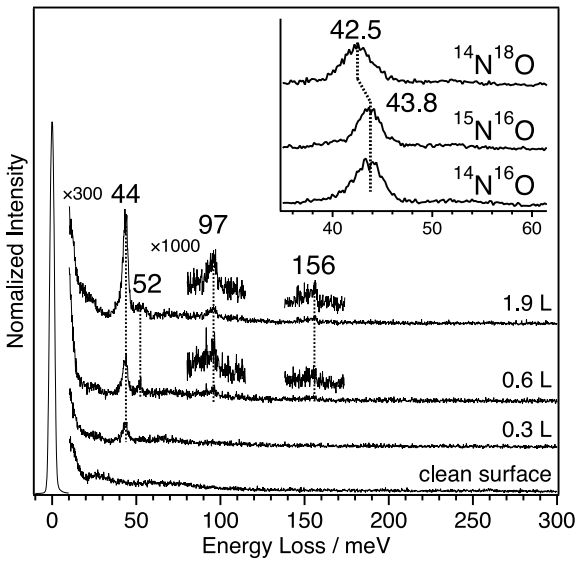

Fig. 4 EEL spectra of NO/Cu(100) at 100 K as a function of exposure. The spectra are vertically offset for clarity. The inset shows the isotope ($^{14}N^{16}O$, $^{14}N^{18}O$ and $^{15}N^{16}O$) dependence of the 44 meV peak.

3.2 NO dissociation pathway

DFT calculations were conducted to elucidate the details of the reaction process. We first considered the reaction pathway for a NO monomer to dissociate directly into N and O atoms at Cu(100) (Fig. S2). The activation barrier for the NO dissociation was found to be 1.11 eV, which is too high to be overcome at ∼100 K. The barrier originates from relatively large adsorption energy of the N atom on the surface. On the other hand, we found that the NO dissociation takes place via the $(NO)_2$ mediated mechanism with the effective activation energy of 0.32 eV, which is significantly smaller than that for the monomer dissociation (Fig. 5) and those for the NO dissociation via $(NO)_2$ on Cu(111) and on Cu(211) of 0.84 eV[51] and 0.62 eV,[52] respectively.

The $(NO)_2$ mediated dissociation proceeds as follows: Two separate NO molecules (Fig. 5A) first form a dimer with the activation energy of 0.17 eV at the nearest neighbor hollow sites (a_0-$(NO)_2$, Fig. 5B). The a_0-$(NO)_2$ is less stable than monomer by 0.09 eV, consistent with the STM observation that the NO monomer rather than the dimer is dominant on the surface (Fig. 2). The a_0-$(NO)_2$ shifts to form an upright ONNO species (Fig. 5C), which then is converted into a flat-lying ONNO species (Fig. 5D), in which O atoms interact directly with the surface Cu atoms. The conversion to this flat configuration requires the activation energy of 0.21 eV, and the flat-lying ONNO is 0.23 eV more stable than the upright ONNO. Subsequently, the flat-lying ONNO reacts to form N_2O and O atom with the activation energy of 0.19 eV (Fig. 5E). The formation of N_2O is followed by the N_2O desorption (Fig. 5F) or N_2O dissociation to form adsorbed O atom and desorbed N_2 (Fig. 5G). The former reaction is endothermic and requires the activation energy of 0.21 eV, while the latter takes place spontaneously, and therefore, the N_2O dissociation may be the predominant path. However, in the $(NO)_2$ dissociation process, significant energy of 1.22 eV is released from the transition state (TS(D-E) in Fig. 5) to the final state (E in Fig 5), suggesting that the released energy can be used to overcome the activation barrier of N_2O desorption. To see which of the two paths, namely, N_2O desorption or dissociation, is dominant, we additionally performed *ab initio* molecular dynamics (AIMD) simulations in the microcanonical ensemble, starting from the transition state of $(NO)_2$ dissociation (Fig. 5TS(D-E)) as done in ref.[33]. In the AIMD simulation, the initial velocities were randomly generated and scaled so that the average kinetic energy became 80 K. The total simulation time was 1 ps, with a 1 fs time step. We found that during the AIMD simulation, spontaneous N_2O desorption takes place (Fig. 6), leaving an O atom on the surface, indicating the importance of dynamical effect. Our AIMD result is consistent with STM observation where the flat-lying ONNO is converted to an O atom adsorbed on the surface (Figs. 3(b) and S3). Here we emphasize that formation of the flat-lying ONNO is crucial and plays the essential role in the NO dissociation on Cu(100). It is noted that the minority molecular state remained after heating to 85 K (Fig.3c), supporting the reaction mechanism via NO dimer; the reaction rate of the second-order process is significantly reduced as the coverage decreases.

3.3 STM-induced reaction at low temperature and intermolecular interaction

To gain further insight into NO dissociation, the reaction was induced and observed stepwise by STM at 6 K[53]. The intermolecular distance was reduced nominally to $2a_0$ ($2a_0$-$(NO)_2$) and $\sqrt{a}_0$ ($\sqrt{a}_0$-$(NO)_2$) and imaged as in Figs. 7a and b, respectively. The a_0-$(NO)_2$ is formed at the nearest neighbor distance, where the image shows twin protrusions (Fig. 7c). The images are reproduced by the STM simulations shown in Figs. 7f-h. The rings appear to be overlapped and the appearance is modified as the distance is varied. The overlap suggests electronic coupling between the molecules[53] as discussed below.

The a_0-$(NO)_2$ (Fig. 7c) was induced to react by applying a voltage pulse with STM. As a consequence, it is converted into a depression of semicircle shape (Fig.7d). Another voltage pulse was applied to the depression, which resulted in the reaction to form a dark spot (Fig. 7e). The sequential reaction induced by STM is shown in Fig. S3, which reveals the registry of the products (depressions) with the surface lattice. The final dark spot is the same as those observed in Fig. 3, and is assigned to the O atom. The simulated STM image for the flat-lying ONNO is shown in Fig. 7i, which well reproduces the semicircle depression in Fig. 7d. Therefore, the sequential reaction observed here supports that the flat-lying ONNO is an intermediate to the dissociation of $(NO)_2$. We repeated the STM-induced reaction of 30 a_0-$(NO)_2$, where half of them were induced to react to form the flat-lying ONNO species, while the others were detached to yield two separate monomers. Thus, we propose that the dissociation of NO at ∼70 K takes place via flat-lying ONNO species, as induced and observed by STM at 6 K; It has too short life time to be observed at ∼70 K.

In the literature, the reactions of NO on low-index Cu surfaces have been studied, and the N-O dissociation has been observed

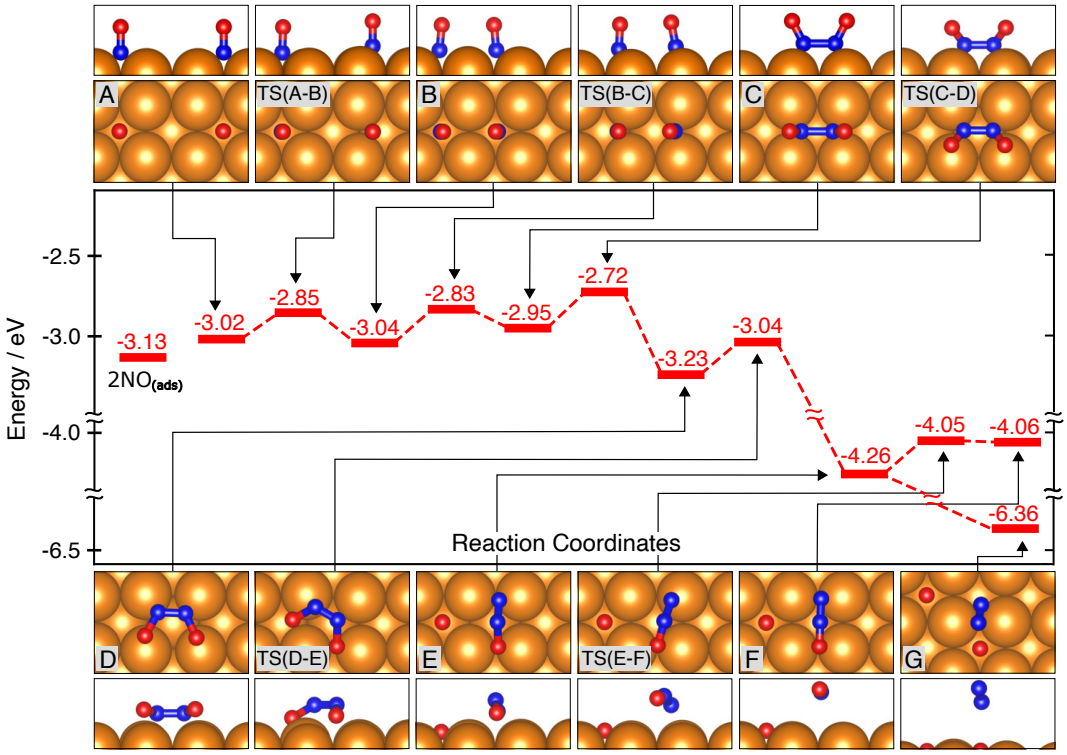

Fig. 5 Optimized reaction pathway of the NO dissociation mediated by NO dimer formation. The adsorption energy per $(NO)_2$ (in eV) is labeled in each state. The energy is referenced to the sum of total energies of clean Cu(100) and two gas-phase NO molecules. Cu, N, and O atoms are represented by orange, blue, and red spheres, respectively.

to occur at different temperature depending on the surface structures. The $(NO)_3$ forms on Cu(111) at 100 K[23] and dissociates above 170 K.[11] On Cu(110), the flat monomer is dominant at low coverage at 110 K, which dissociates at ∼140 K.[24] Compared to these results, the dissociation of NO on Cu(100) occurs at exceptionally low temperature (∼70 K). Because it has not been observed either on Cu(111) or Cu(110), we propose that the flat-lying ONNO is a key intermediate that facilitates the NO dissociation on Cu(100).

The dimer formation is found to be an essential process in the reaction of NO. As the intermolecular distance decreases, the rings of individual molecules are modified, as shown in Figs. 7a, b and c, suggesting that the overlap of the orbitals causes the formation of the bonding- ($7a_1$ and $2b_1$) and antibonding-type ($2a_2$ and $7b_2$) orbitals.[53] To understand the mechanism of the electronic coupling, we calculated the density of states (PDOS) projected onto the molecular orbitals (MO) of the NO dimer as a function of intermolecular distance (Fig. S4). The degenerate $2\pi^*$ states of the NO monomer are located in the vicinity of the Fermi level (Fig. 8a and Fig. S4a), which result in the ring-shape protrusions in the STM image[41]. As the intermolecular distance becomes smaller, the $2\pi^*$ orbitals start to interact, yielding the dimer orbitals ($7a_1$, $2b_1$, $2b_1$ and $7b_2$). At the distance of $2\sqrt{2}a_0$ (Fig. S4b), the PDOSs for two NO molecules the surface are almost identical to those of the monomer, indicating negligible orbital interaction. As the distance is reduced to $2a_0$ (Fig. S4c) and $\sqrt{2}a_0$ (Fig. S4d), the orbital interaction develops and the $7b_2$ state dominates near the Fermi level. The corresponding experimental and simulated STM images show node-like features, i.e., depressions between the two rings, as clearly seen in Figs. 7b and g, implying the antibonding interaction between NO molecular orbitals. At the distance of a_0 (Fig. S4e), the interaction between σ orbitals becomes much stronger, resulting in the much larger splitting between $7a_1$ (σ) and $7b_2$ (σ^*) orbitals. At this distance, $2b_1$ (π) and $2a_2$ (π^*) orbitals dominate in the vicinity of the Fermi level,[41] resulting in the elongated twin protrusions in the STM image (Figs. 7c and h). We note that although there is almost no enthalpy gain in dimer formation as shown in Fig. 5, the electronic states are perturbed even at relatively large intermolecular distance of $2a_0$ (∼5Å, Fig. S4c). Such long-range interaction suggests that it is mediated by the surface,[54] and is related to the coverage dependence of the electronic states of NO on metal surfaces.

3.4 Origin of the formation and reaction of the flat-lying ONNO

Once formed, the a_0-$(NO)_2$ (Fig. 5B) diffuses to the bridge site and is transformed into the upright ONNO (Fig. 5C). The upright ONNO then rotates to form the more stable flat-lying ONNO (Fig. 5D), which plays a key role in the NO dissociation. We evaluated the intermolecular and molecule-substrate interaction energies (Table S1), and found that for the upright ONNO, the molecule (ONNO)-substrate interaction becomes slightly weaker than the a_0-$(NO)_2$. However, when the ONNO is flipped and adsorbs in the flat-lying configuration, the intermolecular (NO-NO) interaction becomes much weaker, while ONNO-substrate

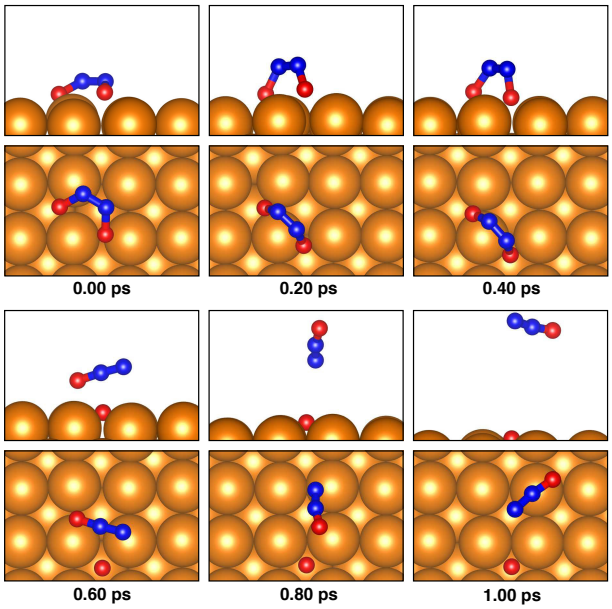

Fig. 6 Snapshots from the AIMD trajectory of N_2O desorption/dissociation, starting from TS(D-E) in Fig. 5TS(D-E).

interaction becomes significantly stronger, resulting in stronger adsorption. In the flat-lying ONNO, the N-N distance is 1.33 Å, which is significantly shorter than that of the gas phase dimer (2.01 Å) and close to that of gas phase N_2O (1.15 Å), suggesting that the ONNO formation triggers the N-N bond formation. Furthermore, the N-O bond length is 1.33 Å, much larger than that of 1.24 Å in the a_0-$(NO)_2$, implying that the N-O bond is weakened and N-O dissociation is facilitated.

To investigate the electronic origins of the stability of the flat-lying ONNO and N-O dissociation, we performed the PDOS analysis. As the N-N bond is formed in the upright ONNO, two NO $2\pi^*$ states hybridize significantly as indicated by their splitting in PDOS ($7a_1$ and $7b_2$ states, Fig. 8c), which is much larger than that of the a_0-$(NO)_2$. This significant hybridization of the MOs of NO molecules in the ONNO dimer is confirmed by the COOP analysis between molecules (Fig. S5). The orbital hybridization is further enhanced in the flat-lying ONNO (Fig. 8d), which results in the fully occupied $2\pi^*$-derived $7a_1$ and $2b_1$ states. Because the $2\pi^*$ orbital of NO is antibonding in nature, this causes the weakening of N-O bond as well as the strengthening of $(NO)_2$ substrate interaction, leading to the NO dissociation on the surface. We note that the ONNO species with such short N-N bond length (1.33 Å) is unstable in the gas-phase, despite the large hybridization of $2\pi^*$ orbitals. The local fourfold structure of Cu(100) may be crucial to form the flat-lying ONNO with a direct N-N bond, which acts as a precursor to the NO dissociation.

4 Conclusions

The elementary process of NO dissociation on Cu(100) was studied by STM, EELS and DFT. The ONNO in a flat configuration was found to be a key intermediate to the dissociation. This intermediate is specific to Cu(100), making this surface exceptionally reactive toward NO compared to other low-index Cu surfaces.

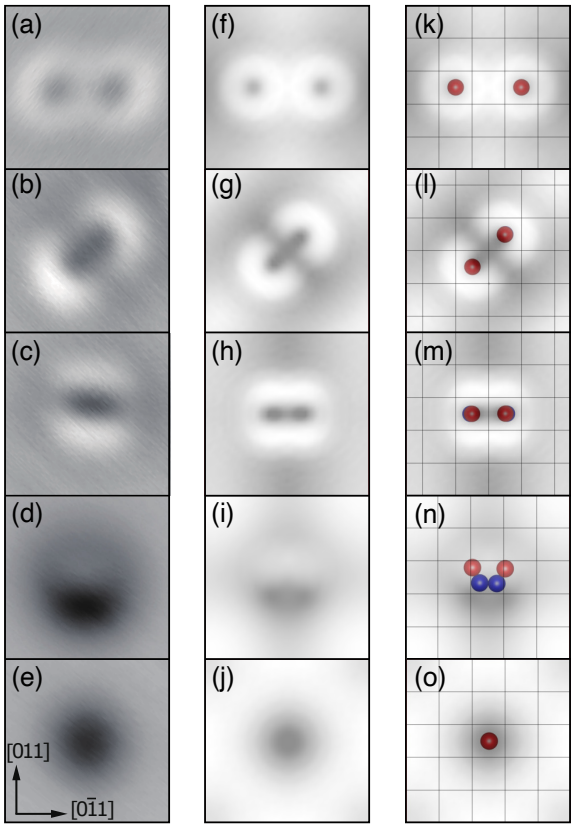

Fig. 7 (a)-(e) A series of experimental STM images of two NO molecules which react to produce an oxygen atom on the surface. The images were obtained at 6 K. Two NO molecules at the distance of (a) $2a_0$, (b) $\sqrt{2}a_0$ and (c) a_0. (d) A semicircle depression produced by STM-induced reaction from a_0-$(NO)_2$ in (c). This is assigned to the flat-lying ONNO dimer. (e) A dark spot produced by STM-induced reaction from the flat-lying ONNO in (d). This is assigned to an oxygen atom. (f)-(j) Simulated STM images corresponding to (a)-(e), respectively. (k)-(o) Simulated STM images overlayed with the corresponding atomic models. Blue and red spheres represent N and O atoms, respectively. The image size of (a)-(e) is 13×12 Å. The images were obtained at V_s=0.1 V and their appearance did not essentially depend on the bias polarity.

In addition, we observed long-range electronic coupling between NO molecules on the surface, which also plays an important role in the $(NO)_2$ and ONNO formation. The present work provides a microscopic insight into the structure dependence of heterogeneous catalysis.

5 Author contributions

K.K. conducted STM and EELS experiments. M.R.A. conducted the DFT calculations and wrote the manuscript. T.N.P., Y.W., Y.H., K.I., Y.M. helped and advised on the DFT calculations. A.S., S.H., T.A. helped with research design and advice on the experiments. H.O. and I.H. supervised the project, provided advice and wrote the manuscript.

Conflicts of interest

There are no conflicts to declare.

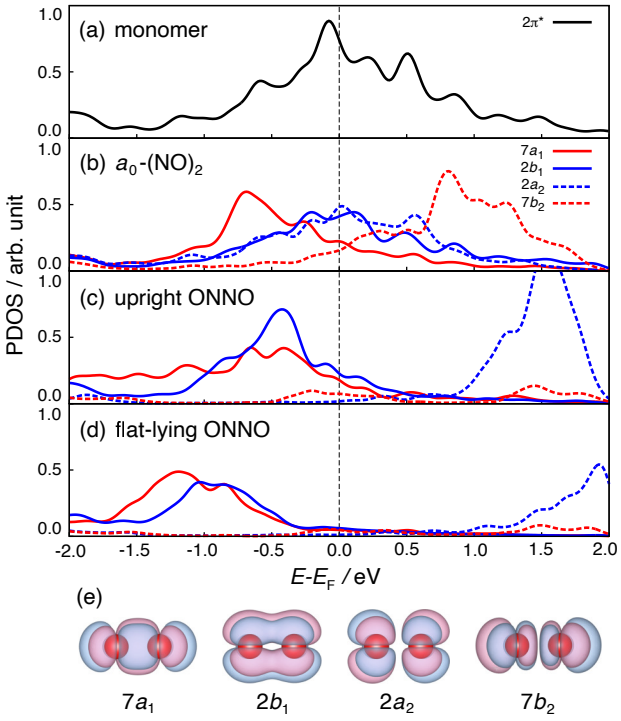

Fig. 8 Projected densities of states (PDOS) onto (a) the $2\pi^*$ orbital for NO monomer on Cu(100), PDOSs onto the molecular orbitals consisting of $2\pi^*$ orbitals ($7a_1$, $2b_1$, $2a_2$, and $7b_2$) for (b) a_0-$(NO)_2$, (c) upright ONNO, and (d) flat-lying ONNO. (e) $7a_1$, $2b_1$, $2a_2$, and $7b_2$ orbitals of $(NO)_2$ in the gas phase.

Acknowledgements

This work was supported by Grants in Aid for Scientifc Research (C) (No. 18K05030) and Scientific Research (B) (No. JP20H02569) and Transformative Research Areas "Hyper-Ordered Structures Science" (Grant No. 20H05883) from the Japan Society for the Promotion of Science (JSPS), and by the Elements Strategy Initiative for Catalysts and Batteries (JPMXP0112101003) supported by the Ministry of Education, Culture, Sports, Science, and Technology, Japan (MEXT), and JST, CREST Grant Number JPMJCR20R4, Japan. M.R.A. acknowledges the financial supports by Indonesia Endowment Fund for Education (LPDP) from the Ministry of Finance of Indonesia. Part of the numerical calculations were performed using the Super Computer facility at Institute for Solid State Physics, the University of Tokyo.

Notes and references

1 J. L. Gland and B. A. Sexton, *Surface Science*, 1980, **94**, 355 – 368.
2 W. A. Brown and D. A. King, *The Journal of Physical Chemistry B*, 2000, **104**, 2578–2595.
3 C. M. Kim, C.-W. Yi and D. W. Goodman, *The Journal of Physical Chemistry B*, 2002, **106**, 7065–7068.
4 R. J. Behm and C. R. Brundle, *Journal of Vacuum Science & Technology A*, 1984, **2**, 1040–1041.
5 A. Ludviksson, C. Huang, H. Jänsch and R. Martin, *Surface Science*, 1993, **284**, 328 – 336.
6 J. Wendelken, *Applications of Surface Science*, 1982, **11-12**, 172 – 185.
7 E. K. Baldwin and C. M. Friend, *The Journal of Physical Chemistry*, 1985, **89**, 2576–2581.
8 S. K. So, R. Franchy and W. Ho, *The Journal of Chemical Physics*, 1989, **91**, 5701–5706.
9 R. Masel, E. Umbach, J. Fuggle and D. Menzel, *Surface Science*, 1979, **79**, 26 – 38.
10 C. Nelin, P. Bagus, J. Behm and C. Brundle, *Chemical Physics Letters*, 1984, **105**, 58 – 63.
11 P. Dumas, M. Suhren, Y. Chabal, C. Hirschmugl and G. Williams, *Surface Science*, 1997, **371**, 200 – 212.
12 W. A. Brown, R. K. Sharma, D. A. King and S. Haq, *The Journal of Physical Chemistry*, 1996, **100**, 12559–12568.
13 A. Shiotari, H. Koshida and H. Okuyama, *Surface Science Reports*, 2021, **76**, 100500.
14 A. Shiotari, *Reactivity of Nitric Oxide on Copper Surfaces: Elucidated by Direct Observation of Valence Orbitals*, Springer, Singapore, 2017.
15 A. Bogicevic and K. Hass, *Surface Science*, 2002, **506**, L237 – L242.
16 Y. Wang, D. Zhang, Z. Yu and C. Liu, *The Journal of Physical Chemistry C*, 2010, **114**, 2711–2716.
17 W. A. Brown, P. Gardner and D. A. King, *The Journal of Physical Chemistry*, 1995, **99**, 7065–7074.
18 W. A. Brown, P. Gardner, M. P. Jigato and D. A. King, *The Journal of Chemical Physics*, 1995, **102**, 7277–7280.
19 C. I. Carlisle and D. A. King, *The Journal of Physical Chemistry B*, 2001, **105**, 3886–3893.
20 Z.-P. Liu, S. J. Jenkins and D. A. King, *Journal of the American Chemical Society*, 2004, **126**, 7336–7340.
21 N. Takagi, K. Ishimura, H. Miura, T. Shishido, R. Fukuda, M. Ehara and S. Sakaki, *ACS Omega*, 2019, **4**, 2596–2609.
22 A. Shiotari, S. Hatta, H. Okuyama and T. Aruga, *The Journal of Chemical Physics*, 2014, **141**, 134705.
23 H. Koshida, H. Okuyama, S. Hatta and T. Aruga, *The Journal of Chemical Physics*, 2016, **145**, 054705.
24 A. Shiotari, T. Mitsui, H. Okuyama, S. Hatta, T. Aruga, T. Koitaya and J. Yoshinobu, *The Journal of Chemical Physics*, 2014, **140**, 214706.
25 M. P. Seah and W. A. Dench, *Surf. Interface Anal.*, 1979, **1**, 2.
26 L. Vattuone, L. Savio and M. Rocca, *High Resolution Electron Energy Loss Spectroscopy (HREELS): A Sensitive and Versatile Surface Tool*, Springer, Berlin, 2013.
27 S. Andersson, B. Persson, T. Gustafsson and E. Plummer, *Solid State Communications*, 1980, **34**, 473–476.
28 Y. Morikawa, K. Iwata and K. Terakura, *Applied Surface Science*, 2001, **169-170**, 11 – 15.
29 Y. Morikawa, H. Ishii and K. Seki, *Phys. Rev. B*, 2004, **69**, 041403.
30 S. E. M. Putra, F. Muttaqien, Y. Hamamoto, K. Inagaki, I. Hamada and Y. Morikawa, *The Journal of Chemical Physics*, 2019, **150**, 154707.

31 J. I. Enriquez, F. Muttaqien, M. Michiuchi, K. Inagaki, M. Geshi, I. Hamada and Y. Morikawa, *Carbon*, 2021, **174**, 36 – 51.

32 F. Muttaqien, Y. Hamamoto, I. Hamada, K. Inagaki, Y. Shiozawa, K. Mukai, T. Koitaya, S. Yoshimoto, J. Yoshinobu and Y. Morikawa, *The Journal of Chemical Physics*, 2017, **147**, 094702.

33 F. Muttaqien, H. Oshima, Y. Hamamoto, K. Inagaki, I. Hamada and Y. Morikawa, *Chem. Commun.*, 2017, **53**, 9222–9225.

34 T. N. Pham, M. Sugiyama, F. Muttaqien, S. E. M. Putra, K. Inagaki, D. N. Son, Y. Hamamoto, I. Hamada and Y. Morikawa, *The Journal of Physical Chemistry C*, 2018, **122**, 11814–11824.

35 T. N. Pham, Y. Hamamoto, K. Inagaki, D. N. Son, I. Hamada and Y. Morikawa, *The Journal of Physical Chemistry C*, 2020, **124**, 2968–2977.

36 D. Vanderbilt, *Phys. Rev. B*, 1990, **41**, 7892–7895.

37 J. c. v. Klimeš, D. R. Bowler and A. Michaelides, *Phys. Rev. B*, 2011, **83**, 195131.

38 G. Román-Pérez and J. M. Soler, *Phys. Rev. Lett.*, 2009, **103**, 096102.

39 J. Wu and F. Gygi, *The Journal of Chemical Physics*, 2012, **136**, 224107.

40 Y. Hamamoto, I. Hamada, K. Inagaki and Y. Morikawa, *Phys. Rev. B*, 2016, **93**, 245440.

41 A. Shiotari, H. Okuyama, S. Hatta, T. Aruga, M. Alducin and T. Frederiksen, *Phys. Rev. B*, 2016, **94**, 075442.

42 G. Mills, H. Jónsson and G. K. Schenter, *Surface Science*, 1995, **324**, 305 – 337.

43 G. Henkelman, B. P. Uberuaga and H. Jónsson, *The Journal of Chemical Physics*, 2000, **113**, 9901–9904.

44 R. Hoffmann, *Rev. Mod. Phys.*, 1988, **60**, 601–628.

45 H. Aizawa and S. Tsuneyuki, *Surface science*, 1998, **399**, L364–L370.

46 Y. Hamamoto, S. A. Wella, K. Inagaki, F. Abild-Pedersen, T. Bligaard, I. Hamada and Y. Morikawa, *Phys. Rev. B*, 2020, **102**, 075408.

47 J. Tersoff and D. R. Hamann, *Phys. Rev. Lett.*, 1983, **50**, 1998–2001.

48 J. Tersoff and D. R. Hamann, *Phys. Rev. B*, 1985, **31**, 805.

49 T. N. Pham, Y. Hamamoto, K. Inagaki, D. N. Son, I. Hamada and Y. Morikawa, *The Journal of Physical Chemistry C*, 2020, **124**, 2968–2977.

50 N. Sheppard and C. De La Cruz, *Phys. Chem. Chem. Phys.*, 2010, **12**, 2275.

51 K. G. Papanikolaou and M. Stamatakis, *Catal. Sci. Technol.*, 2021, **11**, 3681–3696.

52 F. Xing, J. Jeon, T. Toyao, K.-i. Shimizu and S. Furukawa, *Chem. Sci.*, 2019, **10**, 8292–8298.

53 A. Shiotari, Y. Kitaguchi, H. Okuyama, S. Hatta and T. Aruga, *Phys. Rev. Lett.*, 2011, **106**, 156104.

54 P. Han and P. S. Weiss, *Surface Science Reports*, 2012, **67**, 19–81.